Northumbria Research Link

Effect of Nanofiller Morphology on the Electrical Conductivity of Polymer Nanocomposites

Qichen Fang[a] and Khalid Lafdi [a,b]

(a) Chemical and Materials Engineering
Department University of Dayton, Dayton, OH 45469-USA

(b) Department of Mechanical and Construction Engineering, Northumbria University, Newcastle upon Tyne, UK

Abstract

Conductive polymers and nanocomposites have attracted great attention in industry and academia for their tremendous potential applications. Most of the research was focused on the type and amount of nano-additives used and fewer on their morphology which is critical in forming the conductive network. In this paper, a detailed investigation of the effect nanomaterial's morphology was carried out to study their electrical conductivity properties. Silver nanowire (AgNW) nanocomposite and silver nanoparticle (AgNP) nanocomposite were fabricated. The morphology, crystallinity, and orientation of various silver nanofillers were characterized. AgNW based nanocomposites have shown a lower percolation threshold. A conductive unit based model was established to explain the evolution of the conductive network and aggregation. The aggregation geometry of nanofiller appeared as a dominant factor in altering the percolation behavior.

1. Introduction

Conductive polymer nanocomposites exhibit excellent electrical conductivity [1,2] and lightweight [3], which have attracted great interest to be used as strain sensor [4-5], biosensors [6], transparent electrodes [7-9], and surface-enhanced Raman scattering (SERS) for plasmonic applications [10]. Conductive nanofiller played an essential role in affecting nanocomposite conductivity. For silver-based nanofiller, the significant

difference in structural and geometrical features between different nanofiller will bring distinct differences in nanofiller network structure and thus the nanocomposites' electrical conductivity. Two types of silver-based nanomaterials were intensively studied: silver nanoparticle (AgNP) with spherical shape and silver nanowire (AgNW) with cylindrical morphology. Recently, AgNW has been studied for the flexible transparent thin film [11-16]. The major differences between AgNP and AgNW are their geometry and specific surface area.

Silver nanomaterials can be easily synthesized by a simple polyol reduction process [17-20]. Depending on reactants concentration [21], thermal condition [22], and the stirring rate [23-25]. The geometry and aspect ratio can be well controlled [26]. AgNP can be considered as a zero-dimensional material. The diameter ranges from 5 nm to 200nm [27-29]. AgNW is a typical one-dimensional cylindrical rod. The diameter varies from 20nm to 200nm, and its aspect ratio ranges from 100 to 2000 based on synthesis conditions [30-32]. As a result, AgNP has a much higher specific surface area than AgNW, and it is easier for AgNW to form a conductive network [33]. The distribution of nanoparticles can be highly affected by the process method [34], thus easily affect the network. The formation of a conductive network is the key in nanocomposite based conductive applications, such as flexible electronics, sensors, electromagnetic interference shielding [35-37]. In conductive nanowire based nanocomposites, the interactions between nanowire and matrix and their dispersion are critical for establishing an active conductive network pathway.

Soheil et al. studied the effect of nano additive geometry in carbon-based materials. They compared multiwall carbon nanotube (MWCNT) and graphene nanoribbon (GNR) nanocomposites and found that GNR nanocomposites have lower conductivity than MWCNT nanocomposite since GNR cannot interlace between each other tightly [38].

Nuha et al. showed that the carbon nanotube (CNT) based nanocomposites have a much higher conductivity than the carbon black (CB) one at the same concentrations [39]. Hongjin mentioned that AgNP could enhance silver-based nanocomposite conductivity by creating a more conductive path [40]. The alignment of nanowires is an important parameter as well. Silver nanowire conductive films can have a dominant alignment by controlling viscosity and evaporation rate [41].

Computational modeling is an alternative way to understand and predict the property of derived nanocomposites [42-43]. With the help of supercomputing methods in recent years, realistic simulation of large scale and multi-body problems becomes faster and more accessible, such as modeling the formation of a percolation network. Xiao et al. developed a model to explain the percolation characteristics of ZnO nanoparticle in composite dielectrics. The model illustrates the formation of the conductive pathway in nanocomposite [43]. In Takuya's study, a novel morphological model was used to understand the importance of CNT aggregation and electron tunneling [44]. The effect of electron tunneling in nanocomposite's conductivity was dominant. Bao et al. clarified that the electron tunneling was affected by polymer film's thickness between nanofiller, thus the contact resistance [45]. In Daewoo Suh's study, after adjusting the distance between silver and silicone and enabled the electron tunneling, nanocomposite's electrical conductivity increased by ~5 orders of magnitude without nanofiller's coalescence [46]. Nuha et al. systematically studied the effect of carbon nanofiller's geometry, aspect ratio, aggregation, and concentration. Their modeling result shows that the conductivity evolution versus nano-additive concentration is profoundly affected by the degree of aggregation. They also revealed that well-dispersed nanofillers are not always preferred for the formation of conductive networks. However, the threshold percolation measured is in a vertical direction rather than an in-plane

direction. The effect of the nanowire's anisotropic distribution was not well modeled, and the mechanism of particle aggregation's effect was not well illustrated. [39].

In this study, the effect of different nanofillers on the formation of conductive networks in an in-plane direction was compared experimentally and numerically. Nanocomposite films were made using the spin coating method. To study the distribution of nanofillers in nanocomposite, the crystallinity and orientation of different silver nanofillers were measured using X-ray diffraction (XRD) methods. A numerical simulation was carried out to better understand the effect of nanofillers' geometry and concentration. A conductive unit based model was established to expound the effect of size and aggregation geometry on the evolution of the conductive network.

2. Experimental section

2.1 Materials

Polyacrylonitrile (PAN, acrylonitrile-co-methyl acrylate copolymer, acrylonitrile content 94%, Mw=100000) was purchased from Scientific Polymer Inc. N, N-Dimethylformamide (DMF, anhydrous, $\geq$99.8%), Anhydrous ethylene glycol (EG, $\geq$99.8%), silver nitrate (AgNO3, Reagent plus, $\geq$99.0%), Polyvinylpyrrolidone (PVP, powder, MW=55000) were purchased from Sigma-Aldrich. Acetone was purchased from Alfa Aesar. Copper(II) Chloride Dihydrate (CuCl$_2$, $\geq$99.8%) was purchased from Acros Organics. All chemicals were used with no further purification.

2.2 Preparation of AgNWs and AgNPs

AgNWs and AgNPs were synthesized separately by a polyol reduction method. In the AgNWs synthesis, 150ml EG was added in a 250ml three flask and heated at 150 ℃ by flask heating mantles. The stir bar was then added with a spin rate of 260 rpm. A thermometer was used at various times to measure the solution's temperature. At 1.5h,

0.16 mL of CuCl$_2$ solution (20 mM, in EG) was added in the flask. After 20 minutes, 5 mL of PVP solution (0.882 M, in EG) was injected into a heated solution, followed by 5 mL of AgNO$_3$ solution (0.564 M, in EG). The reaction ended at 1.5h, and the solution was cooled at room temperature. 100ml Acetone was added to the product to dilute the solution. Furthermore, the products were centrifuged at 4000 rpm for 30 min. After washing the products twice with acetone, the final AgNWs were stored in acetone. Acetone can prevent the aggregation of AgNWs and will participate in the manufacturing of conductive composite. The synthesis of AgNPs was carried out similarly. The major difference was that no CuCl$_2$ was added, the PVP concentration was 0.932 M in EG, and the concentration of AgNO$_3$ was 0.72 M in EG.

2.3 Preparation of PAN nanocomposite

The weight of the nanofiller was well controlled. Before mixing the nanofiller with PAN, 1 g PAN was added in 9 g DMF. With a stir bar added, the PAN/DMF solution was stirred while maintaining a temperature of 65 ℃. After 12h, the solution of PAN/DMF was well prepared. For a 20 vol% mixture of silver nanofiller and PAN, 0.6 g of silver nanofiller was added. The silver nanofiller was soaked in acetone, and the silver precipitated after 1 minute. Then 2.7 g of PAN/DMF solution was added using a pipette. By weighting the final solution, more acetone could be added to adjust the weight ratio of PAN and DMF to be 1:2. In the final mixture, there was 0.6 g of silver nanofiller, 0.27 g of PAN, 2.43 g of DMF, and 1.22 g of acetone. After stirring at 180 rpm for 1 hour, a homogenous solution was obtained. The formation of aggregates could occur if the stirring time was too long. The dispersed solution was used right after the preparation. A Speed line P2604 spin coater was used to fabricate the thin film. 0.2 ml dispersed solution was added on the glass and then spun at 2000 rpm for 15 seconds. After the spin coater stopped, the thin film was transferred to a 60 ℃ oven immediately.

After 30 minutes, a well-cured film was obtained. The processing scheme is shown in Figure 1.
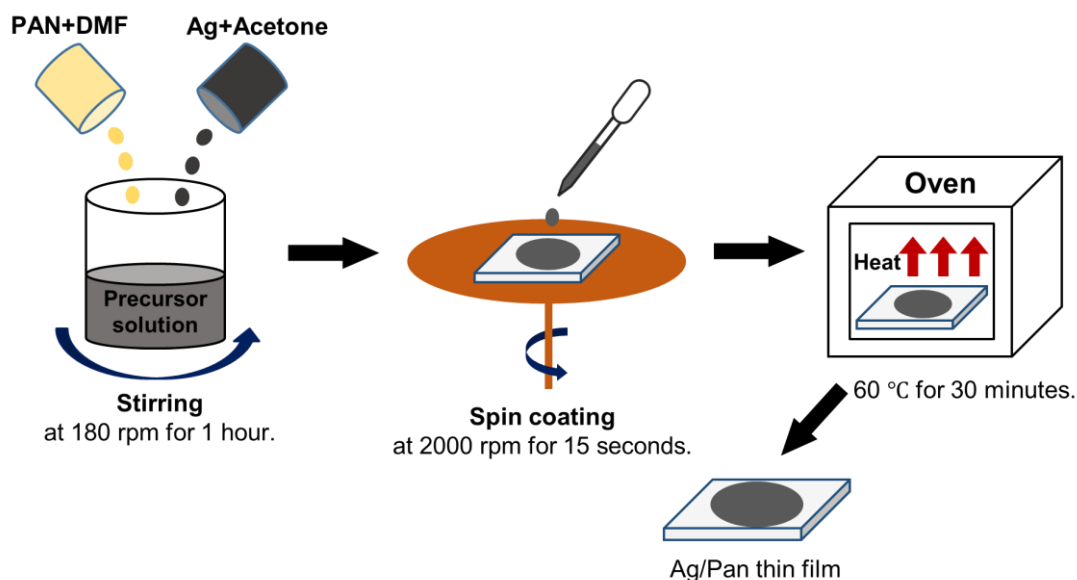

Figure 1. Schematic illustration of the preparation of the Ag/PAN thin film.

2.4 Characterization

The morphology of the AgNWs and AgNPs were characterized using a Phenom desktop SEM (15kv, Pro X, Phenom). The thickness of nanocomposites was characterized using TMA (Q400, TA universal) with an expansion probe at room temperature. Weight percentage was obtained by burning the nanocomposite with a TGA (Q500, TA universal) and then converted to volume percentage. The electrical conductivity of thin films was measured using the four-probe method (Loresta-GP MCP-T610). The wide-angle X-ray diffraction (WAXD, Smartlab X-ray diffractometer, Rigaku) was used to characterize the nanofiller crystallinity, and small-angle diffraction (2D-XRD, Oxford Diffraction Xcalibur 3 x-ray diffractometer) patterns were used to determine the orientation of thin films [47].

2.5 Numerical method

The simulation consisted of two steps. The first step was to construct the 3D geometry of the thin film and randomly generate the nanoparticle inside. The second step was to

analyze the network after all nanoparticles were generated. The quantum tunneling effect was considered as the main factor affecting electrical conductivity [46,48]. The length of a junction between nanofillers determined if the wire or particle was connected to the network. It was assumed that nanofillers could not cross each other. The shape of AgNWs was considered a cylinder, and the shape of AgNP was considered a sphere. According to the measurement of Ag nanoparticle and Ag nanowire, the parameters of two nanofillers were set as follows in the simulation. The diameter of each AgNW was 150 nm. The average length of AgNW is 18 ± 5 µm, so the length of AgNW was any value between 13 to 23 µm. The geometry of every AgNP was about a 200 nm diameter sphere. The simulation was carried out with MatLab [39].

The minimal length between two nanofillers was calculated and determined as the key parameter for analyzing the network. The minimum distance function (Eqn(1)) was applied in the calculation. The parameter V and W in the function was the two-point on the nanowire axis segment, shown in Figure 2.

$$a, b, c, d, V, W \in \mathrm{R}^n$$

$$v, w \in \mathrm{R}$$

$$V = \{v \times b + (1 - v) \times a | 0 \le v \le 1\}$$

$$W = \{w \times b + (1 - w) \times a | 0 \le w \le 1\}$$

The distance of (*V*, *W*)

$$= \sqrt{\sum_{i=1}^{n}(v \times b_i + (1 - v) \times a_i - w \times c_i - (1 - w) \times d_i)^2} \qquad \text{Eqn (1)}$$
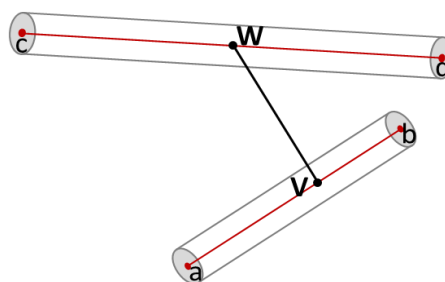

Figure 2. Minimal distance calculation.

In order to ensure every particle or wire was compliant with the rules, the flow chart was shown in the source file, figure s1. The primary purpose of analyzing the network was to determine if a conductive network was formed or not.

3 Results and discussion

3.1 Morphology.

Figure 3 showed the image of AgNP (Figure 3a) and AgNW (Figure 3b). The average size of a single AgNP was 200 nm. AgNW had an average length, and the diameter was 18 ± 5 μm and 150 nm. As observed via SEM, the aggregation of silver nanofiller was distinct because the nanofiller was stored in acetone [49]. After sonication and mixing with DMF, most large aggregates were eliminated. In order to eliminate unfavorable aggregation, nanofillers were used right after being synthesized. However, the AgNP would still disperse as small aggregate in the polymer solution, shown in source file figure s4.
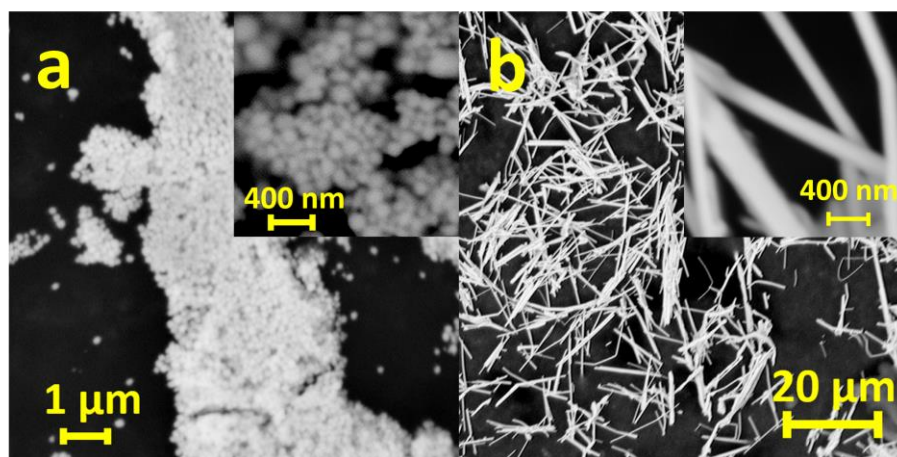

Figure 3. SEM images of (a) AgNP and (b) AgNW nanofiller.

The electrical network was dictated by the silver nanofiller's dispersion in PAN. A careful inspection of the nanocomposite at different vol% was critical in understanding the percolation formation. Figures 4a and 4b showed the surface of AgNP/PAN at 7 vol% and 18 vol%. Most AgNPs were embedded in the polymer matrix. As vol%

increased, the number of AgNPs increased visibly. Meanwhile, there was no electrically conductive network observed at 18 vol%. A closer inspection of the AgNP/PAN revealed less interaction among particles, shown in figure 4a. Figure 4c and 4d showed the surface of PAN/AgNW at 9 vol% and 17 vol%. In those figures, it could be observed that most AgNWs were separated, and aggregates were removed. At 9 vol%, the silver nanowires overlapped each other and formed a complete network. As vol% increased, the overlapping of each AgNW also increased, and the conductive network gradually formed. When vol% increased to 17 vol%, a complete nanowire network can be distinctly observed. The nanofillers' dispersion was evident.

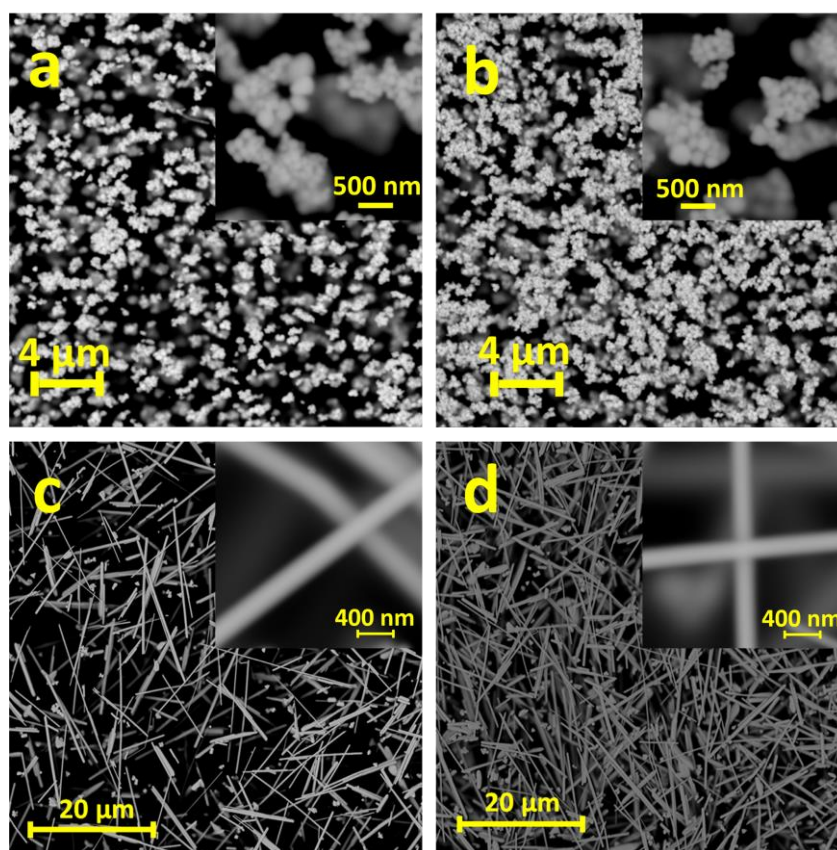Figure 4. SEM images of (a) 7 vol% AgNP/PAN, (b) 18 vol% AgNP/PAN, (c) 9 vol% AgNW/PAN, and (d) 17 vol% AgNW/PAN.

The sample thickness was 6 μm, and the AgNWs were dispersed in three dimensions within the nanocomposite. Meanwhile, the spin coating process resulted in a smooth

surface because the vertical nanowires would settle and flatten out during spinning. Most AgNWs were embedded in the PAN matrix. Only a small amount of AgNWs was exposed to the surface. As AgNWs were embedded tightly in cured PAN, which created an electrically conductive network.

3.2 XRD Results

Since silver was the nanofiller, its orientation within the nanocomposite gave more insight into understanding its electric conductivity. The silver nanofillers were synthesized, and a wide-angle XRD was used to characterize the AgNP and AgNW nanofiller structure. In Figure 5a, the XRD results showed four prominent peaks corresponded to (111) at 38.1°, (200) at 44.4°, (220) at 64.5°, (311) at 77.4°, which agreed with a published report from Jyoti et al. [50]. A very sharp (111) peak was evident at 38.1° for AgNP and AgNW. As more silver atoms attached to the (111) plane and AgNW grew in the [110] direction (Figure 5b), high orientation was observed [51].
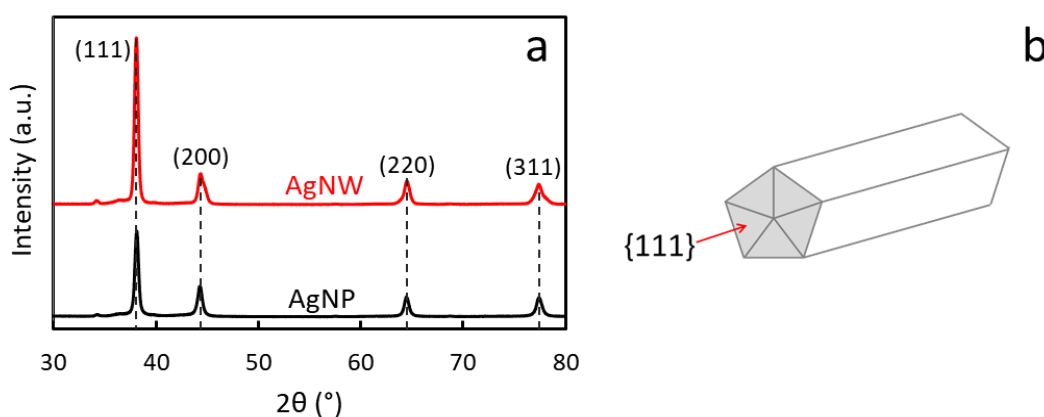
Figure 5. (a) XRD patterns, and (b) Illustration for AgNW growth

In order to prove the orientation of nanowires in the film, the incident X-ray was shot through the film (in-plane direction), and the 2D detector collected the diffracted information, shown in Figure 6a, b. The AgNW was embedded in PAN after spinning. The average length of AgNW (18 ± 5μm) was more than the thickness of derived

nanocomposites (6 μm). In Figure 6d, distinct orientations were visible, which was influenced by the AgNW length, nanocomposite thickness, and the processing method. Compared to the AgNW sample, the ring of the AgNP sample (Figure 6c) was continuous. The four arcs were attributed to the (111), (200), (220), (311) peak (shown in Figure 5a). The intensity of each arc was confirmed with the XRD result, especially for AgNP. At a certain thickness of the film, far smaller than the length of the nanofiller, longer AgNW leads to a higher orientation.
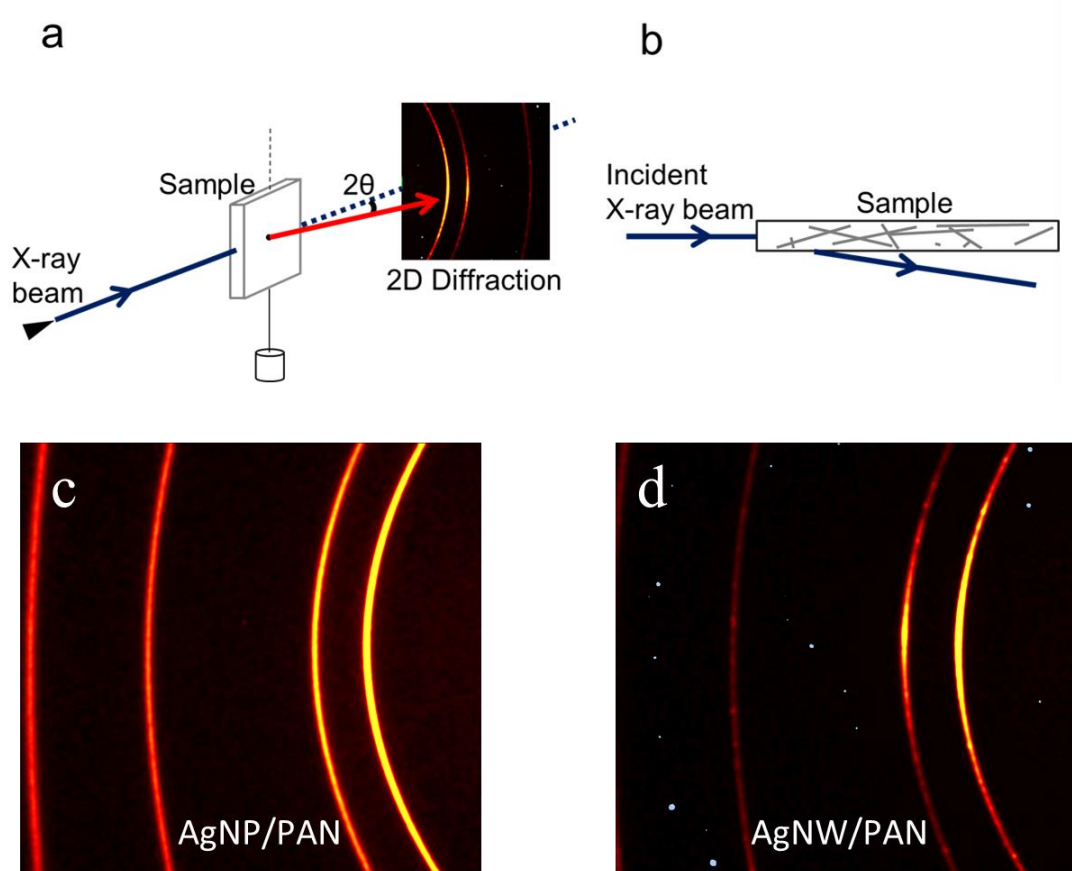
Figure 6. (a)Schematic of the 2D-XRD. (b) Illustration of the X-ray beam diffraction. (c) 2D-XRD pattern for AgNP/PAN, and (d) AgNW/PAN film.

3.3 Experimental electrical Conductivity and modeling results.

The film was thin (6 μm) and elastic. Peeling it from the slide could easily make a permanent deformation, affecting electrical conductivity [52]. So after the sample was taken out of the oven, further electrical measurements were conducted on the film slide.

A four-point probe method was used to measure electrical conductivity. Measurements were conducted at five different places for each sample (and five times per place). The final conductivity was the average value of the data. Figure 7a showed the nanocomposites' electrical conductivity as a volume percentage for AgNW/PAN film. With TGA amended, the volume percentage of AgNW was from 9.2 to 18.6 vol%. As the 7 vol% AgNW/PAN film was not conductive, a sharp increase was observed from 9.2 to 10.6 vol%. It was possible to determine that 9.2 vol% was near the percolation threshold.
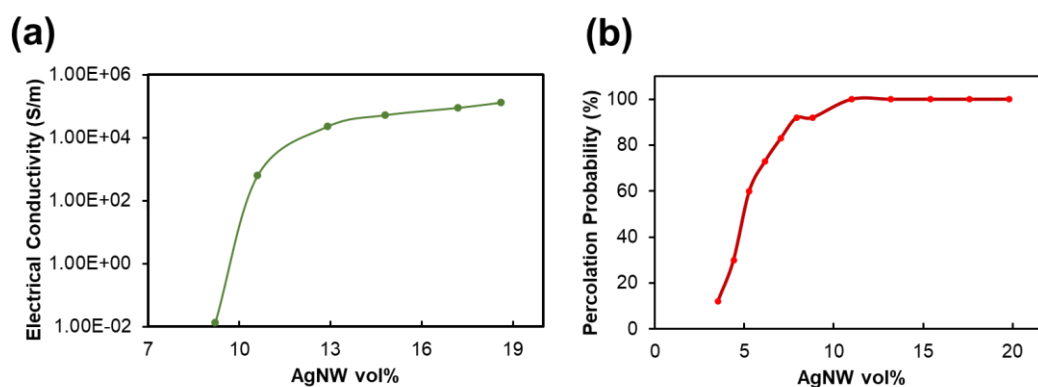
Figure 7. (a)Electrical conductivity at various volume percentages of AgNW. (b), Percolation probability *vs.* AgNW vol%.

Moreover, percolation could be affected by wire distribution dispersion [53]. The percolation threshold was hard to find on the experimental result, but the trend was evident. The electrical conductivity measurement of 0.011 S/m at 9.2 vol% suggested that a conductive network was established. Therefore, the percolation threshold should be below 9.2 vol%. Below the percolation threshold, the nanowires' concentration dominantly affects the percolation formation, thus the conductivity. After the percolation threshold, the tunneling effect mainly influences conductivity [54].

A percolation probability simulation was used to understand the sharp change in

conductivity better. Silver nanowires in the simulation volume were presented in the source file, figure s2. The results were collected from 600 simulations, 50 simulations for each vol%. In the simulation, the number of nanowires generated was determined by the volume percentage. The simulation results were shown in Figure 7b. As the number of nanowires increased, the percolation success probability increased. Only 12% of simulations showed percolation success at 3.5 vol%. At 7.0 vol%, 82% of simulations showed percolation success. 18% of the sample can be treated as an insulator. In other words, nanowires were partially networked at this amount, and some nanowires were still segregated. As vol% increased to 8.8 vol%, 92% of simulations showed percolation success. After generating more nanowires in the model, at 11 vol%, more conductive pathways were formed and resulted in high electrical conductivity. If more nanowires were added after this amount, more nanowires could be connected and would smoothly increase the electrical conductivity. Another finding could explain the sharp increase of conductivity: as the AgNW vol% increased linearly, the wire interactions increased exponentially, shown in the source file, figure s3. After the volume percentage exceeded 9 vol%, long connectivity was achieved, the intersections of the nanowires increased exponentially, which decreased the resistance. Overall, it is possible to conclude that the sharp change of electrical conductivity was mainly due to a percolation probability of 90% being achieved.

Compared to the AgNW/PAN film, the AgNP/PAN film was not conductive even at 29.6 vol%. A very low conductivity, which was 0.52 S/m, was measured at 54.4 vol% of AgNP/PAN. After increasing the AgNP volume to 61.9 vol%, the conductivity increased to 34.4 S/m, which was lower than AgNW/PAN film at 10.6 vol%. The lower conductivity of AgNP/PAN could be caused by the contact resistance between the particles [55-56]. The contact resistance of the AgNP/PAN film was too high to be

measured. Typically, smaller particle size results in a lower percolation threshold [52]. 200 nm AgNP used in this study was bigger than other studies that are focusing on AgNP based conductive nanocomposite [57-58]. For example, Muhammed et al. used 77 nm AgNP to make an electrically conductive nanocomposite fiber in their study [57]. It was hard to determine AgNP/PAN's percolation threshold from the experiment results because of the low conductivity. Therefore, we performed an aggregation theory based simulation for AgNP/PAN in the next section. However, there was a significant difference between AgNP/PAN and AgNW/PAN on conductivity. The effect of morphology on electrical conductivity was evident.

4. Influence of particle geometry

It is important to clarify how the geometry of particles affects the conductive network's formation. A mathematical model was established to understand the aggregation situations of nanoparticles in Figure 8. We applied this model to explain the excellency of nanowire compared to the spherical nanoparticles, in other words, AgNW vs. AgNP. Experimental results showed that AgNP/PAN film could not achieve electrical conductivity until 15 vol%. However, the AgNW/PAN film could form a conductive network at 9 vol%. The property of nanoparticle-based nanocomposite was highly dependent on its aggregation structure. For example, a CB based high-structure could form a conductive network more efficiently than the low-structure one [59-60]. However, the mathematical approach of the percolation mechanism was not well developed. Consequently, quality control and empirical methods were the only tools for the industry in production [61].

4.1 Conductive unit model

We established a model for understanding the formation efficiency of conductive networks, as illustrated in Figure 8. We assumed the conductive network consists of

similar units: the conductive unit (the yellow circle). In this case, a smaller conductive network based on the tunneling effect always existed inside this conductive unit. We assumed the number of conductive nanoparticles inside a single conductive unit was the same for a better comparison. From left to right, the degree of aggregation increased. Figure 8, from top to bottom, the number of nanoparticles increased.

For the well-dispersed conductive unit, particles were close to each other. As a result, this unit was conductive but not as efficient as other conformations. When slightly aggregated, some of the nanoparticles attracted each other and formed a dendritic structure. When the nanoparticles were highly aggregated, most nanoparticles attracted each other and formed a bar-like structure. While n=20, the increments of size on three conductive units were different, the size of well-dispersed conductive units increased little, and the highly-aggregated aggregate increased the most. While n=30, the difference in size increment between the three types of conductive units were much more dominant. The bars' structure in highly aggregated conductive units could be regarded as nanowire, and the conductive units were like a low aspect ratio nanowire cluster. This phenomenon could be concluded as the following. The addition of nanoparticles was mostly "wasted" everywhere in the well-dispersed scenario, and the size of the conductive unit changed little. The additional nanoparticles were attached to the branch for the slightly aggregated scenario, and the rest were dispersed. The size of the conductive unit changed more than the well-dispersed. The additional nanoparticles were attached straightly on the formed bars for the highly aggregated scenario or form new bars. In both ways, the size of the conductive unit was significantly increased. As shown in Figure 8, the excess part's size was defined as "h" and the $h_4 > h_2 > h_3 > h_1$. With the number of nanoparticles increases, the aggregate size was dominantly affected by the aggregation degree.

Based on this model, with the same number of particles, the highly aggregated conductive unit trends to be larger. For a certain size, the highly-aggregated conductive unit needed fewer particles to form a conductive network inside. Furthermore, with the same size of the conductive unit, the highly-aggregated conductive unit tended to form a larger conductive network in the nanocomposite. Nanowire could be considered as a special case of the highly-aggregated conductive unit. For example, the silver nanowire aspect ratio was over 100 in this study, and the AgNW could be regarded as 100 stacked AgNP. Practically, the AgNW nanocomposite achieved electrical conductivity at a lower threshold than the AgNP nanocomposite [61].

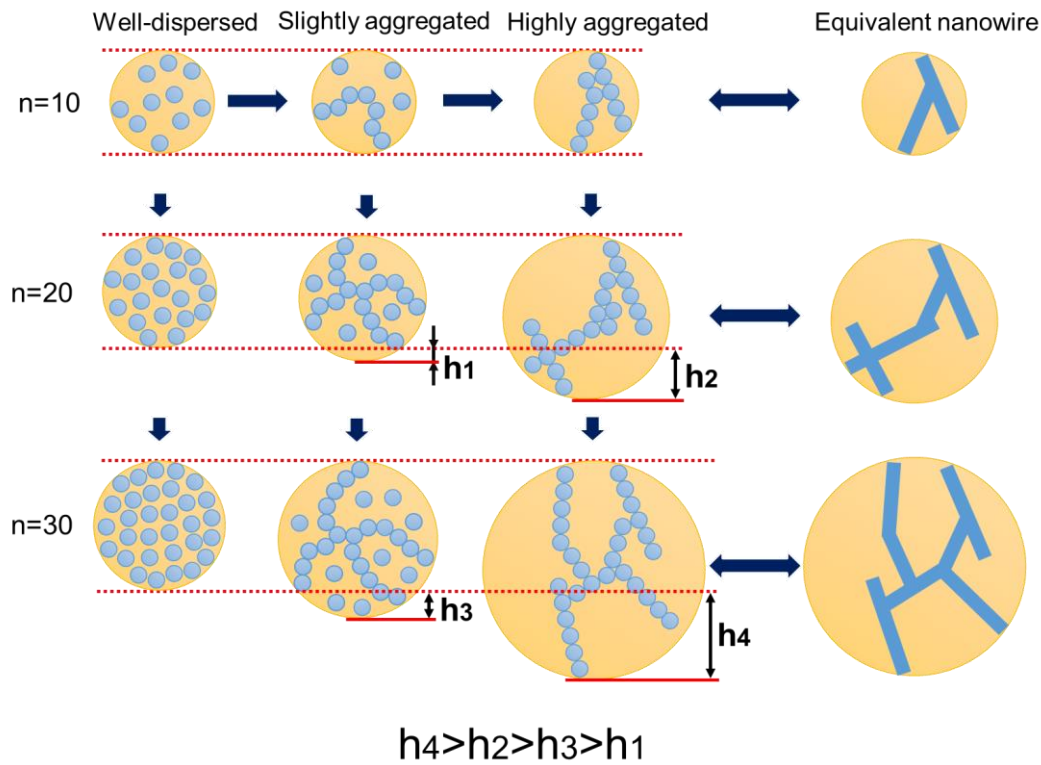

Figure 8. Evolution of aggregate model for well-dispersed, slightly-aggregated, highly-aggregated, and equivalent nanowire.

4.2 Simulation on aggregation.

In Figure 4a, the irregular shape of the AgNP aggregates was evident. They may cause

some anisotropic property and eventually influence network formation. Generally, the silver nanoparticles have a percolation threshold of around 5 to 20 vol% [61]. Therefore, the simulation of 20 vol% of AgNP/PAN was used to study the influence of aggregate geometry on the percolation. As the previous section mentioned, the diameter of AgNP was 0.2μm. In the first 100 simulations, we considered the silver nanoparticles were very well dispersed, and every particle stayed alone in the 3×3×3 cube, and 1289 particles were generated, as shown in Figure 9a. The red bar in the cube represented the directly connected particle. With AgNW/PAN's experimental data, a valid connection was considered as the distance between each particle was smaller than 0.03 μm. No percolation was shown after 100 simulations.

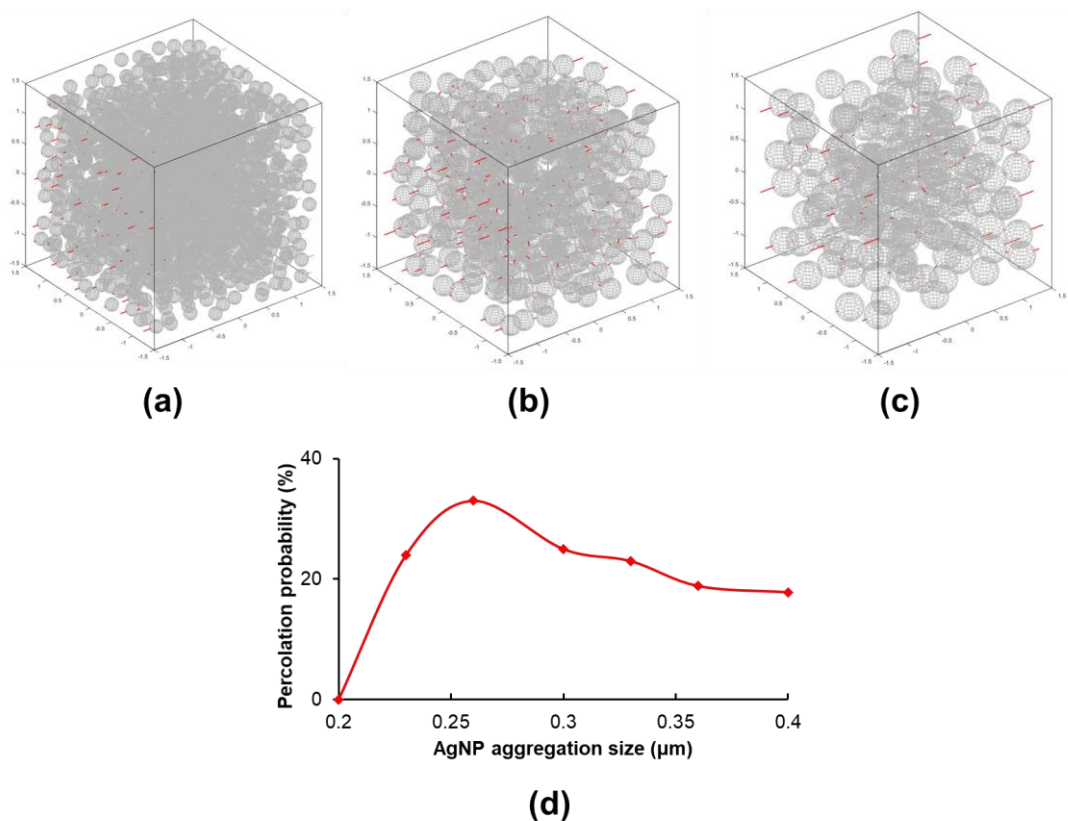(a)   (b)   (c)

(d)

Figure 9. Simulation of aggregates size is (a) 0.2 μm, (b) 0.3 μm, and (c) 0.4 μm, (d) AgNP aggregation size *vs.* percolation success

For the 100 simulations shown in figure 9b, we considered the nanoparticles formed

irregular shape aggregates, and the average size of the aggregates is 0.3 μm. In order to have 20 vol% AgNP in the cube, the particle volume was expanded 3.375 times compare to 0.2 μm particle's, and the generating particle number decreased to 382. Even as little as two silver particles can form an irregular aggregation, it will increase the real particle number. In order to simplify the simulation, the least particle number was used. In figure 9b, each particle in the cube was considered to be a 0.3μm irregular aggregate. 25 of 100 simulations showed successful percolation. Interestingly, after each irregular aggregate's size increased to 0.4μm, only 18 of 100 simulations showed successful percolation. A percolation of 0.4μm silver aggregates was shown in figure 9c. More simulations on various AgNP aggregation sizes were made, and the trend was obtained. Out of 100 simulations, the percolation probability dramatically increased first and then decreased with the aggregates' size increased, shown in figure 9d. The percolation probability reached the maximum value 33% at 0.26 μm and then decreased to 18% at 0.4 μm.

With the increase of successful percolation followed, the increase of conductive unit size could be expounded. First, with the anisotropism of the conductive unit, the difficulties in forming a conductive network decreased. Second, based on our model, the size of the conductive unit increased little. It required less conductive unit for a conductive network, which implied the network's formation more efficiently. However, the effect of the anisotropic property was dominant at this scale. With the aggregation size increased, the nanoparticle aggregate needed more nanoparticles to fill the space. As a result, the size of the conductive unit increased a little bit. The decrease of successful conductive simulation could be explained as the aggregate number decrease became much influential. Thus, bigger nanoparticle aggregates would increase the difficulty in forming a conductive network.

4.3 Validation of the model

The extension of this model confirmed previous studies well. For instance, electrical conductivity evolved differently with three distinct particle morphologies, as shown in figure 10: well-dispersed nanoparticle, high structure nanoparticle, and nanowire. In the well-dispersed scenario, more nanoparticles were consumed to extend the conductive unit size. Therefore, the conductive threshold of AgNP/HDPE nanocomposites in figure 10a is as high as 17 vol% (~68wt%) [62]. CB aggregates were aggregated into high-structure in figure 10b. Expanding the size of conductive units would consume fewer particles. The CB/HDPE had a low threshold of 2.7 wt% (1.35 vol%) [59]. In Figure 10c, the conductive threshold of CNT/PLLA nanocomposite was as low as 0.6 vol% (1.2 wt%) [63]. The nanotube consumed the least "nanoparticles" to extend the conductive unit size. In conclusion, particles' geometry had a significant effect on affecting network formation, and our model provided a novel insight into this subject.
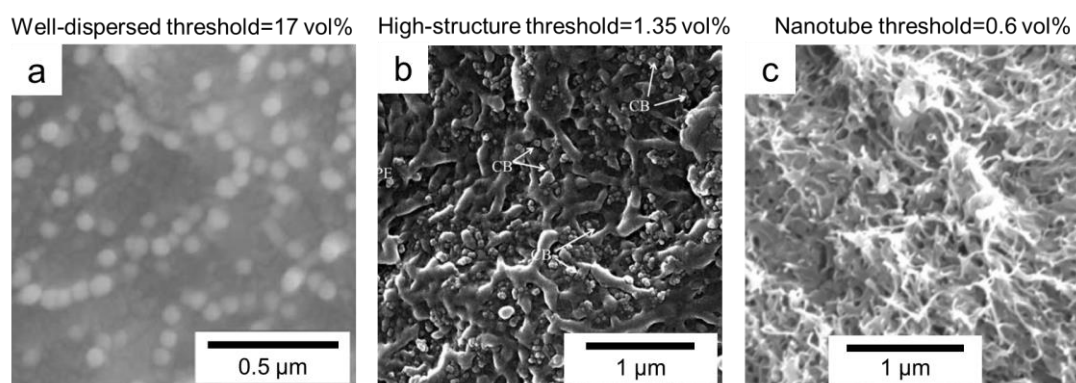

Figure 10. SEM image of (a)well dispersed structure of AgNP/HDPE nanocomposite [62]; (b) high structure of CB/HDPE nanocomposite [59]; (c) nanotube connection of CNT/PLLA nanocomposite [63].

5. Conclusions

In this study, AgNW/PAN and AgNP/PAN were characterized, and differences were observed in the percolation behavior. These differences were attributed to the nanofiller

geometry. The experimental result showed that the electrical conductivity increased with the volume percentage increase above 9.2 vol% for AgNW/PAN. The percolation threshold for AgNW/PAN was around 8-9 vol%. The AgNP/PAN exhibited a very low conductivity at 55 vol%. This result was expected because the larger size of AgNP would have a higher critical volume fraction, and the contact resistance between AgNP was very high.

For both nanocomposites, the simulation results agreed with the experimental data. Depending on the simulation result, the sharp increase in conductivity after the percolation threshold seems mainly affected by the increasing percolation probability and exponential increase of wire intersections. Another important finding was that the geometry of the aggregation of AgNP was the dominant factor in altering the percolation. The irregular shape of the aggregates would add an anisotropic property to the nanocomposites. As the size of the aggregates increased, the number of aggregates decreased at a certain concentration. By increasing the critical fraction, the formation of the conductive network was hindered. A conductive unit based geometrical model was established to understand the complex aggregation behavior of nanoparticles. Such a model was successfully applied to explain the experimental and simulation results.

Notes

The authors declare no competing interests.

Reference

1 Walker, S. Brett, and Jennifer A. Lewis. "Reactive silver inks for patterning high-conductivity features at mild temperatures." *Journal of the American Chemical Society* 134, no. 3,(2012), 1419-1421.

2 Alshehri, Ali H., Malgorzata Jakubowska, Anna Młożniak, Michal Horaczek, Diana Rudka, Charles Free, and J. David Carey. "Enhanced electrical conductivity of silver nanoparticles for high frequency electronic applications." *ACS applied materials & interfaces* 4, no. 12 (2012): 7007-7010.

3 Zhan, Chuanxing, Guoqiang Yu, Yang Lu, Luyan Wang, Evan Wujcik, and Suying Wei. "Conductive polymer nanocomposites: a critical review of modern advanced devices." Journal of Materials Chemistry C 5, no. 7 (2017): 1569-1585.

4 Amjadi, Morteza, Aekachan Pichitpajongkit, Sangjun Lee, Seunghwa Ryu, and Inkyu Park. "Highly stretchable and sensitive strain sensor based on silver nanowire–elastomer nanocomposite." ACS nano 8, no. 5 (2014): 5154-5163.

5 Min, S. Han, A. M. Asrulnizam, M. Atsunori, and M. Mariatti. "Properties of stretchable and flexible strain sensor based on silver/PDMS nanocomposites." Materials Today: Proceedings 17 (2019): 616-622.

6 Wanekaya, Adam K., Wilfred Chen, Nosang V. Myung, and Ashok Mulchandani. "Nanowire-based electrochemical biosensors." *Electroanalysis: An International Journal Devoted to Fundamental and Practical Aspects of Electroanalysis* 18, no. 6 (2006): 533-550.

7 Altin, Yasin, Mahmut Tas, İsmail Borazan, Ali Demir, and Ayse Bedeloglu. "Solution-processed transparent conducting electrodes with graphene, silver nanowires and PEDOT: PSS as alternative to ITO." Surface and Coatings Technology 302 (2016): 75-81.

8 Mohammadnezhad, Mahyar, Gurpreet Singh Selopal, Nasser Alsayyari, Rusoma Akilimali, Fabiola Navarro-Pardo, Zhiming M. Wang, Barry Stansfield, Haiguang Zhao, and Federico Rosei. "CuS/graphene nanocomposite as a transparent conducting oxide and pt-free counter electrode for dye-sensitized solar cells." Journal of the Electrochemical Society 166, no. 5 (2018): H3065.

9 Yuksel, Recep, Sahin Coskun, Gorkem Gunbas, Ali Cirpan, Levent Toppare, and Husnu Emrah Unalan. "Silver nanowire/conducting polymer nanocomposite electrochromic supercapacitor electrodes." Journal of The Electrochemical Society 164, no. 4 (2017): A721.

10 Wadhwa, Heena, Devender Kumar, Suman Mahendia, and Shyam Kumar. "Microwave assisted facile synthesis of reduced graphene oxide-silver (RGO-Ag) nanocomposite and their application as active SERS substrate." Materials Chemistry and Physics 194 (2017): 274-282.

11 Ackermann, Thomas, Serhat Sahakalkan, Ivica Kolaric, Engelbert Westkämper, and Siegmar Roth. "Technical requirements, manufacturing processes and cost efficiency for transparent electrodes based on silver nanowires and carbon nanotubes." In *Nanoengineering: Fabrication, Properties, Optics, and Devices XII*, vol. 9556, p. 955602. International Society for Optics and Photonics, 2015.

12 Song, Myungkwan, Dae Sung You, Kyounga Lim, Sujin Park, Sunghoon Jung, Chang Su Kim, Dong-Ho Kim et al. "Highly efficient and bendable organic solar cells with solution-processed silver nanowire electrodes." *Advanced Functional Materials* 23, no. 34 (2013): 4177-4184.

13 Li, Bo, Shengrong Ye, Ian E. Stewart, Samuel Alvarez, and Benjamin J. Wiley. "Synthesis and purification of silver nanowires to make conducting films with a transmittance of 99%." *Nano letters* 15, no. 10 (2015): 6722-6726.

14 Zhang, Ye, Jiangna Guo, Dan Xu, Yi Sun, and Feng Yan. "One-pot synthesis and purification of ultralong silver nanowires for flexible transparent conductive electrodes." *ACS applied materials & interfaces* 9, no. 30 (2017): 25465-25473.

15 Cho, Seungse, Saewon Kang, Ashish Pandya, Ravi Shanker, Ziyauddin Khan, Youngsu Lee, Jonghwa Park, Stephen L. Craig, and Hyunhyub Ko. "Large-area cross-aligned silver nanowire electrodes for flexible, transparent, and force-sensitive mechanochromic touch screens." *Acs Nano* 11, no. 4 (2017): 4346-4357.

16 Ricciardulli, Antonio Gaetano, Sheng Yang, Gert-Jan AH Wetzelaer, Xinliang Feng, and Paul WM Blom. "Hybrid Silver Nanowire and Graphene-Based Solution-Processed Transparent Electrode for Organic Optoelectronics." *Advanced Functional Materials* 28, no. 14 (2018): 1706010.

17 Korte, Kylee E., Sara E. Skrabalak, and Younan Xia. "Rapid synthesis of silver nanowires through a CuCl-or CuCl 2-mediated polyol process." *Journal of Materials Chemistry* 18, no. 4 (2008): 437-441.

18 Sun, Yugang, Byron Gates, Brian Mayers, and Younan Xia. "Crystalline silver nanowires by soft solution processing." *Nano letters* 2, no. 2 (2002): 165-168.

19 Tao, Andrea, Prasert Sinsermsuksakul, and Peidong Yang. "Polyhedral silver nanocrystals with distinct scattering signatures." *Angewandte Chemie International Edition* 45, no. 28 (2006): 4597-4601.

20 Wiley, Benjamin, Yugang Sun, Brian Mayers, and Younan Xia. "Shape-controlled synthesis of metal nanostructures: the case of silver." *Chemistry–A European Journal* 11, no. 2 (2005): 454-463.

21 Ran, Yunxia, Weiwei He, Ke Wang, Shulin Ji, and Changhui Ye. "A one-step route to Ag nanowires with a diameter below 40 nm and an aspect ratio above 1000." *Chemical communications* 50, no. 94 (2014): 14877-14880.

22 Sun, Yugang, Yadong Yin, Brian T. Mayers, Thurston Herricks, and Younan Xia. "Uniform silver nanowires synthesis by reducing AgNO3 with ethylene glycol in the presence of seeds and poly (vinyl pyrrolidone)." *Chemistry of Materials* 14, no. 11 (2002): 4736-4745.

23 Lee, Jinhwan, Phillip Lee, Hyungman Lee, Dongjin Lee, Seung Seob Lee, and Seung Hwan Ko. "Very long Ag nanowire synthesis and its application in a highly transparent, conductive and flexible metal electrode touch panel." *Nanoscale* 4, no. 20 (2012): 6408-6414.

24 Wiley, Benjamin, Thurston Herricks, Yugang Sun, and Younan Xia. "Polyol synthesis of silver nanoparticles: use of chloride and oxygen to promote the formation of single-crystal, truncated cubes and tetrahedrons." *Nano Letters* 4, no. 9 (2004): 1733-1739.

25 Wiley, Benjamin, Yugang Sun, and Younan Xia. "Polyol synthesis of silver nanostructures: control of product morphology with Fe (II) or Fe (III) species." *Langmuir* 21, no. 18 (2005): 8077-8080.

26 Zhang, Pei, Ian Wyman, Jiwen Hu, Shudong Lin, Zhiwei Zhong, Yuanyuan Tu, Zhengzhu Huang, and Yanlong Wei. "Silver nanowires: Synthesis technologies, growth mechanism and multifunctional applications." *Materials Science and Engineering: B* 223 (2017): 1-23.

27 Agnihotri, Shekhar, Soumyo Mukherji, and Suparna Mukherji. "Size-controlled silver nanoparticles synthesized over the range 5–100 nm using the same protocol and their antibacterial efficacy." *Rsc Advances* 4, no. 8 (2014): 3974-3983.

28 Bastús, Neus G., Florind Merkoçi, Jordi Piella, and Victor Puntes. "Synthesis of highly monodisperse citrate-stabilized silver nanoparticles of up to 200 nm: kinetic control and catalytic properties." *Chemistry of Materials* 26, no. 9 (2014): 2836-2846.

29 Hulteen, John C., David A. Treichel, Matthew T. Smith, Michelle L. Duval, Traci R. Jensen, and Richard P. Van Duyne. "Nanosphere lithography: size-tunable silver nanoparticle and surface cluster arrays." *The Journal of Physical Chemistry B*103, no. 19 (1999): 3854-3863.

30 Wang, Shang, Yanhong Tian, Su Ding, and Yilong Huang. "Rapid synthesis of long silver nanowires by controlling concentration of Cu2+ ions." *Materials Letters* 172 (2016): 175-178.

31 Ma, Jingjing, and Maosheng Zhan. "Rapid production of silver nanowires based on high concentration of AgNO 3 precursor and use of FeCl 3 as reaction promoter." *RSC Advances* 4, no. 40 (2014): 21060-21071.

32 Zhang, Kaili, Yongguo Du, and Shimin Chen. "Sub 30 nm silver nanowire synthesized using KBr as co-nucleant through one-pot polyol method for optoelectronic applications." *Organic Electronics* 26 (2015): 380-385.

33 De, Sukanta, Thomas M. Higgins, Philip E. Lyons, Evelyn M. Doherty, Peter N. Nirmalraj, Werner J. Blau, John J. Boland, and Jonathan N. Coleman. "Silver nanowire networks as flexible, transparent, conducting films: extremely high DC to optical conductivity ratios." ACS nano 3, no. 7 (2009): 1767-1774.

34 Al-Ajrash, Saja M. Nabat, Khalid Lafdi, Erick S. Vasquez, Francisco Chinesta, and Philippe Le Coustumer. "Experimental and numerical investigation of the silicon particle distribution in electrospun nanofibers." Langmuir 34, no. 24 (2018): 7147-7152.

35 Liu, Chang, Ivan Sergeichev, Iskander Akhatov, and Khalid Lafdi. "CNT and polyaniline based sensors for the detection of acid penetration in polymer composite." Composites Science and Technology 159 (2018): 111-118.

36 Liu, Chang, Khalid Lafdi, and Francisco Chinesta. "Durability sensor using low concentration carbon nano additives." Composites Science and Technology (2020): 108200.

37 Liu, Chang, and Khalid Lafdi. "Self-Assembly and Surface Tension Induced Fractal Conductive Network in Ternary Polymer System." ACS Applied Polymer Materials 1, no. 3 (2019): 493-499.

38 Sadeghi, Soheil, Mohammad Arjmand, Ivonne Otero Navas, Alireza Zehtab Yazdi, and Uttandaraman Sundararaj. "Effect of nanofiller geometry on network formation in polymeric nanocomposites: Comparison of rheological and electrical properties of multiwalled carbon nanotube and graphene nanoribbon." Macromolecules 50, no. 10 (2017): 3954-3967.

39 Al Habis, Nuha, Chang Liu, Jean-Baptiste Dumuids, and Khalid Lafdi. "Intelligent design of conducting network in polymers using numerical and experimental approaches." RSC Advances 6, no. 97 (2016): 95010-95020.

40 Jiang, Hongjin, Kyoung-sik Moon, Yi Li, and C. P. Wong. "Surface functionalized silver nanoparticles for ultrahigh conductive polymer composites." Chemistry of Materials 18, no. 13 (2006): 2969-2973.

41 Ackermann, Thomas, Raphael Neuhaus, and Siegmar Roth. "The effect of rod orientation on electrical anisotropy in silver nanowire networks for ultra-transparent electrodes." Scientific reports 6 (2016): 34289.

42 Davidson, Ernest R. "Computational transition metal chemistry." (2000): 351-352.

43 Yang, Xiao, Jun Hu, Shuiming Chen, and Jinliang He. "Understanding the percolation characteristics of nonlinear composite dielectrics." Scientific reports 6

(2016): 30597.

44 Morishita, Takuya, Mitsumasa Matsushita, Yoshihide Katagiri, and Kenzo Fukumori. "A novel morphological model for carbon nanotube/polymer composites having high thermal conductivity and electrical insulation." Journal of Materials Chemistry 21, no. 15 (2011): 5610-5614.

45 Bao, W. S., S. A. Meguid, Z. H. Zhu, and G. J. Weng. "Tunneling resistance and its effect on the electrical conductivity of carbon nanotube nanocomposites." Journal of Applied Physics 111, no. 9 (2012): 093726.

46 Suh, Daewoo, K. P. Faseela, Wonjoon Kim, Chanyong Park, Jang Gyun Lim, Sungwon Seo, Moon Ki Kim, Hyungpil Moon, and Seunghyun Baik. "Electron tunneling of hierarchically structured silver nanosatellite particles for highly conductive healable nanocomposites." Nature communications 11, no. 1 (2020): 1-11.

47 Rodriguez-Navarro, Alejandro B. "XRD2DScan: new software for polycrystalline materials characterization using two-dimensional X-ray diffraction." Journal of Applied Crystallography 39, no. 6 (2006): 905-909.

48 Vodolazskaya, Irina V., Andrei V. Eserkepov, Renat K. Akhunzhanov, and Yuri Yu Tarasevich. "Effect of tunneling on the electrical conductivity of nanowire-based films: Computer simulation within a core–shell model." Journal of Applied Physics 126, no. 24 (2019): 244903.

49 Tilaki, R. M., and S. M. Mahdavi. "Stability, size and optical properties of silver nanoparticles prepared by laser ablation in different carrier media." Applied Physics A 84, no. 1-2 (2006): 215-219.

50 Jyoti, Kumari, Mamta Baunthiyal, and Ajeet Singh. "Characterization of silver nanoparticles synthesized using Urtica dioica Linn. leaves and their synergistic effects with antibiotics." Journal of Radiation Research and Applied Sciences 9, no. 3 (2016): 217-227.

51 Yoo, Dae-Hwang, Tran Viet Cuong, Van Hoang Luan, Nguyen Tri Khoa, Eui Jung Kim, Seung Hyun Hur, and Sung Hong Hahn. "Photocatalytic performance of a Ag/ZnO/CCG multidimensional heterostructure prepared by a solution-based method." The Journal of Physical Chemistry C 116, no. 12 (2012): 7180-7184.

52 D'Alessandro, Antonella, Annibale Luigi Materazzi, and Filippo Ubertini. NANOTECHNOLOGY IN CEMENT-BASED CONSTRUCTION. S.l.: PAN STANFORD PUBLISHING, (2019). 303-371.

53 Al-Saleh, Mohammed H., and Uttandaraman Sundararaj. "A review of vapor grown carbon nanofiber/polymer conductive composites." Carbon 47, no. 1 (2009): 2-22.

54 Han, Baoguo, Siqi Ding, and Xun Yu. "Intrinsic self-sensing concrete and structures: A review." Measurement 59 (2015): 110-128.

55 Zhang, Rongwei, Wei Lin, Kyoung-sik Moon, and C. P. Wong. "Fast preparation of printable highly conductive polymer nanocomposites by thermal decomposition of silver carboxylate and sintering of silver nanoparticles." ACS applied materials & interfaces 2, no. 9 (2010): 2637-2645.

56 Zhang, Rongwei, Kyoung-sik Moon, Wei Lin, and C. P. Wong. "Preparation of highly conductive polymer nanocomposites by low temperature sintering of silver nanoparticles." Journal of Materials Chemistry 20, no. 10 (2010): 2018-2023.

57 Liu, Jianguo, Xiangyou Li, and Xiaoyan Zeng. "Silver nanoparticles prepared by chemical reduction-protection method, and their application in electrically conductive silver nanopaste." Journal of Alloys and Compounds 494, no. 1-2 (2010): 84-87.

58 Ajmal, C. Muhammed, Seonghyun Bae, and Seunghyun Baik. "A superior method for constructing electrical percolation network of nanocomposite fibers: In situ

thermally reduced silver nanoparticles." Small 15, no. 1 (2019): 1803255.

59 Ren, Danqi, Shaodi Zheng, Feng Wu, Wei Yang, Zhengying Liu, and Mingbo Yang. "Formation and evolution of the carbon black network in polyethylene/carbon black composites: Rheology and conductivity properties." Journal of Applied Polymer Science 131, no. 7 (2014).

60 Chen, Jianwen, Xihua Cui, Kunyan Sui, Yutian Zhu, and Wei Jiang. "Balance the electrical properties and mechanical properties of carbon black filled immiscible polymer blends with a double percolation structure." Composites Science and Technology 140 (2017): 99-105.

61 Wypych, G. "5-PHYSICAL PROPERTIES OF FILLERS & FILLED MATERIALS." Handbook of Fillers (Fourth Edition): ChemTec Publishing (2016): 303-371.

62 Rybak, Andrzej, Gisele Boiteux, Flavien Melis, and Gerard Seytre. "Conductive polymer composites based on metallic nanofiller as smart materials for current limiting devices." Composites Science and Technology 70, no. 2 (2010): 410-416.

63 Zhang, Kai, Gen-Hui Li, La-Mei Feng, Ning Wang, Jiang Guo, Kai Sun, Kai-Xin Yu et al. "Ultralow percolation threshold and enhanced electromagnetic interference shielding in poly (L-lactide)/multi-walled carbon nanotube nanocomposites with electrically conductive segregated networks." Journal of Materials Chemistry C 5, no. 36 (2017): 9359-9369.